University of BRISTOL

Publisher's PDF, also known as Version of record

Link to published version (if available):
[10.1049/joe.2018.8196](10.1049/joe.2018.8196)

Link to publication record in Explore Bristol Research
PDF-document

University of Bristol - Explore Bristol Research
General rights

IET Journals
The Institution of Engineering and Technology

Sub-assembly experiments to determine PWM supply-induced losses in electric machines

Jonathan Godbehere[1] ✉, Andrew Hopkins[1], David Drury[1], Phil Mellor[1]

[1]University of Bristol, UK
✉ E-mail: jg7560@my.bristol.ac.uk

Abstract: This paper presents a low-cost approach to experimentally characterise the effect of the inverter supply on the losses in an electrical machine. The set-up comprises of representative subassemblies of the stator and winding, referred to as 'motorettes', and a single phase, fast switching silicon-carbide-based converter. The sub-assembly-based thermal analysis has been shown to be a time and cost-effective method to examine winding loss, over a range of operating conditions. In addition to the slot to stator thermal resistance and capacitance. This provides critical information for thermal model calibration and produces more accurate thermal and loss predictions of the full machine behaviour. A test arrangement has been devised to replicate the magnetic excitation of the electrical machine stator during normal operation. This builds upon previous techniques, to allow iron loss to be investigated. Through multiple tests using DC, AC, and PWM-AC supplies, a 20% increase in iron loss is observed due to PWM effects.

1 Introduction

Variable speed control of electric machines requires the use of variable frequency and variable voltage inverters. This is most commonly achieved by pulse width modulation (PWM) voltage control. A consequence of this is the introduction of high-frequency harmonics on top of the fundamental signal. These harmonics in turn lead to additional losses in an electric machine, pre-dominantly as hysteresis and eddy current losses in the iron [1, 2]. Typical iron loss models for electric machines, such as the Steinmetz and Bertotti equations, assume sinusoidal flux density variation. This does not fully represent typical operation with a PWM supply and accurate prediction of iron loss can be challenging.

Experimental analysis has shown that the additional loss induced by a PWM inverter can be significant. In [2], a 50% increase in core loss is measured for a 150-kVA synchronous machine, when supplied from a 2-level, 1 kHz switching frequency inverter. In [3], a 50% increase in iron loss is predicted for an interior permanent magnet (IPM) machine with a PWM supply switching at 10 kHz, and a 112% increase in iron loss at 1 kHz, using the same operating point. The additional iron loss induced in the electric machine due to a PWM supply can vary dramatically. It is a complex phenomenon dependant on many factors, such as the type of machine, winding configuration, iron core loss characteristics, lamination thickness, operating point, switching frequency and number of inverter levels, to name just a few. Accurate prediction of the loss is necessary to allow power-dense and efficient electric machines to be designed and realised.

There is considerable interest in developing iron loss models and simulation techniques which can account for PWM induced loss. However, due to their complex nature, calibration to experimentally obtained results is typically necessary. Several techniques are presented in [1, 4, 5], which study PWM-induced losses in wound components. Techniques based on magnetic flux are derived and then applied to the simulation of an electric machine. However, the flux patterns observed in an electric machine are vastly different to that of the ideal situation in a ring core, reducing the effectiveness of the technique. Other authors have studied the problem using electric machines, such as a stator core in [6] and an IPM machine, without magnets, in [3]. These techniques prove to be effective; however, they cannot be easily applied to a new machine design, different to that studied. On top of this, validating a loss model is difficult, as the high-frequency

PWM loss cannot be accurately measured through voltage and current readings. More advanced techniques are required, such as calorimetry, which is employed in [2].

Here, a new approach is taken. Representative sub-assemblies of the stator and winding are used to develop an experimental approach, to separate out the iron loss from the winding loss. The sub-assembly 'motorettes' are significantly easier and cheaper to produce compared to that of a complete electric machine. However, because they are constructed using the same geometry and materials selected for use in the full machine assembly, they provide a high level of detail directly applicable to the machine design in question. So far in the literature, motorette sub-assemblies have been used to investigate and characterise the thermal model of an electric machine [7], down-select the insulation system to maximise thermal performance [8], and study AC winding loss [9]. Here, thermal modelling techniques are used to isolate the PWM supply-induced loss. Through separate tests with DC, pure AC, and PWM-AC excitation, an accurate thermal model is produced, then used to determine the individual loss components through superposition.

2 Experimental procedure

There are two main challenges to overcome in developing the experimental technique proposed. The first is how to induce iron loss in a sub-assembly, at flux levels representative of that of the complete electric machine. The second challenge is determining the distribution and source of loss within the sub-assembly, i.e. DC winding loss, AC winding loss, iron loss, and PWM supply-induced loss, when only the total loss may be measured. This section will discuss both challenges in turn.

A typical implementation of a motorette uses a single-stator tooth and coil, representative of a concentrated winding machine. Heat extraction via the stator periphery is replicated via a water-cooled cold plate, insulated chamber, and power supply. The total power loss and temperature values within the sample can be recorded at thermal steady state, or over a transient duty cycle. Injecting DC current into a single stator tooth and coil provides detailed information on the thermal performance. However, testing with an AC current does not provide realistic data on AC loss within a machine, Fig. 1.

In Fig. 2, a three-tooth assembly is simulated. The slot leakage flux is now more accurately represented. As the magnetic reluctance across the slots is identical to that in the complete
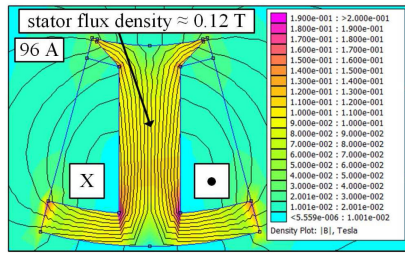
Fig. 1 *2D FEA magneto-static simulation of a single tooth and coil motorette, [10]*
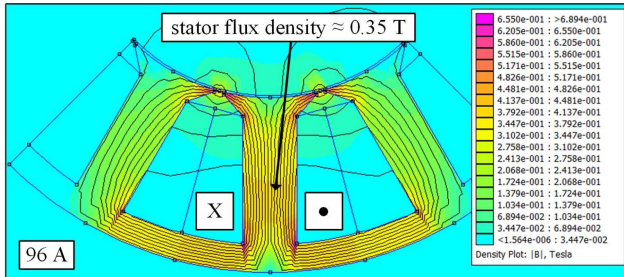

Fig. 2 *2D FEA magneto-static simulation of the triple motorette assembly, central coil energised only [10]*
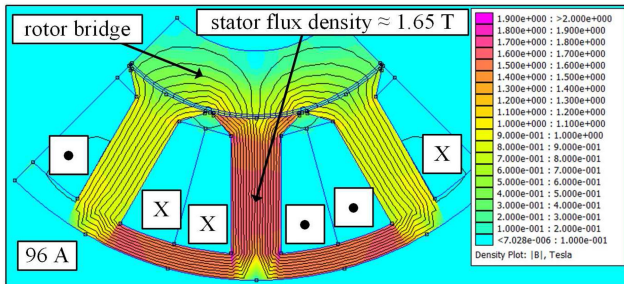

Fig. 3 *2D FEA magneto-static simulation of the triple motorette assembly, with rotor 'keeper' and all coils energised [10]*

machine assembly, the proximity loss is also representative of normal machine operation [9]. However, the peak change in magnetic flux density is relatively small. This means that iron loss present in the sample will not be representative of normal operation.

Finally, the arrangement proposed here is shown in Fig. 3. An iron rotor 'keeper' is placed on top of the stator teeth, and the three coils are connected in series as shown. This is done to achieve the maximum change in flux density possible within the central tooth, which is around 1.65 T at rated current. With this motorette configuration, a significant contribution of iron loss will be observed, alongside DC and AC winding loss. Although the flux density distribution is not fully representative of the rotating field in the complete machine assembly, the arrangement is similar enough to provide useful loss and thermal data for calibrating design models for the complete machine. Simulations may be compared to this simplified scenario, to verify the effect of build factors on loss. It may then be used to investigate phenomenon which are difficult to predict, such as the additional iron loss caused by a PWM switched supply.

Assuming the arrangement presented in Fig. 3 is produced, multiple components of loss will be induced. However, it is desirable to know the distribution of each component. Typically, this is estimated via FEA simulations and compared to the total loss measured. However, this presents a problem if the simulated results do not match the experiments. Here, a procedure is used to match the loss distribution to the predictions of a thermal model and the measured temperature distribution. This method will be discussed in more detail in Section 4.

3 Motorette hardware construction

For the purposes of this study, an existing machine design has been selected. It is based on a 10 pole, 12 slot, PM machine for an automotive application. Full details of the design methodology may be found in [11]; however, the important parameters to this analysis are summarised in Table 1. A double layer, concentrated winding machine, was selected to ensure a fully representative motorette winding configuration could be produced.

The electrical steel used is Cogent NO20, 0.2 mm silicon iron, pre-coated with Rembrandtin Remisol EB 549 epoxy resin. Stacks of electrical steel were produced using a heated press machine, which activates the resin while maintaining the desired stack height. A stacking factor of 97% was achieved.

The motorette teeth and rotor bridge sections were then cut to shape using electrical discharge machining (EDM).

Fig. 4 presents a single motorette sample, before and after winding. The slot liner selected was Nomex 410, 0.25 mm. To provide a detailed description of the thermal performance of the motorettes, a number of type-K thermocouples were placed within each sample. The positions of the thermocouples are presented in Fig. 4, and consist of six separate locations. The tooth and yoke temperatures are K_T, K_{YM} and K_{YS}. A small and shallow hole was drilled to accommodate the thermocouple head, which was then secured using a high temperature super glue. These were placed on both ends of the motorette tooth. K_{ST} and K_{YS} are the temperatures on the radial and tangential interface between the slot and iron. These were secured behind the winding using a high temperature fibre glass tape. Thermocouples were placed in both slots, either side of the tooth. Two thermocouples are present for each separate location. This is to provide a better temperature accuracy and redundancy should a thermocouple fail. The winding was performed as described by the specification in Table 1. The thermocouples (K_{EW}) were then placed on each end-winding.

The motorette samples have been produced in a modular fashion i.e. a single tooth is wound in isolation. The benefit of this is a compact and short end-winding, leading to lower winding loss. To ensure that the three samples sit together correctly on the interface plate, a compression tool was produced. This compressed the windings in both slots against the tooth and held the windings in place during the impregnation process. A non-solvent varnish was used: DOLPHON CC 1105 HTC, and the samples were dip impregnated according to the manufacturer's instructions. Fig. 5 shows three completed motorette samples, positioned on the interface plate. This aluminium interface plate was built to fit the outer stator surface of the motorettes, and emulate cooling via the housing in a conventional radial electric machine. It can be observed in Fig. 5 that the three motorette samples sit together correctly, with minimal gaps between the adjacent teeth or interface plate.

As mentioned previously, the aim of the sub-assembly experiment is to emulate the thermal behaviour seen during normal machine operation. This test set-up is presented in Fig. 6. The motorette samples are positioned on the interface plate, which in turn is attached to a water-cooled cold plate. The motorette winding coils are connected in series, and a current is input into them. Due to the thermally insulated chamber, the main heat flow is from winding to cold plate, through the stator iron and interface plate. The water is regulated to 15°C, and thermal paste is used to improve the thermal conductivity between the motorettes, interface plate, and cooling plate. A 0.8-mm-thick slot liner is used to maintain a constant air gap between the motorette teeth and rotor bridge. A clamp is then used to secure the rotor bridge and motorettes in place during testing, Fig. 7.

4 Test procedure

First, a test with the windings driven from a DC supply is used to calibrate a thermal model of the machine. Under DC excitation the losses are more evenly spread throughout the winding and total loss can be measured to very high accuracy [8]. Next, an AC power supply with low total harmonic distortion is used to characterise the AC loss components under pure sinusoidal excitation. The distribution of loss is then estimated by using the thermal model calibrated in the first step. Finally, tests with a PWM-based AC

Table 1 Motorette and machine parameters

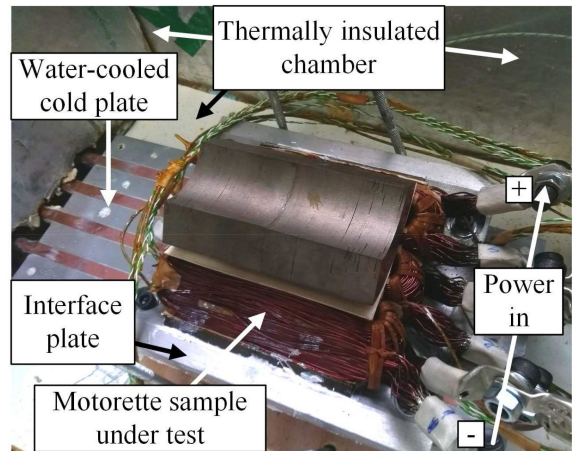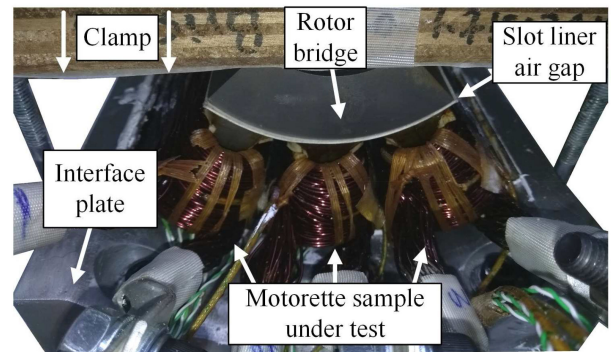| No. poles	No. slots	Peak current, A	Stator bore, mm	Active length, mm	No. turns per coil	Conductor diameter, mm	No. conductors in hand
10	12	96	92.4	90	7	0.8	44
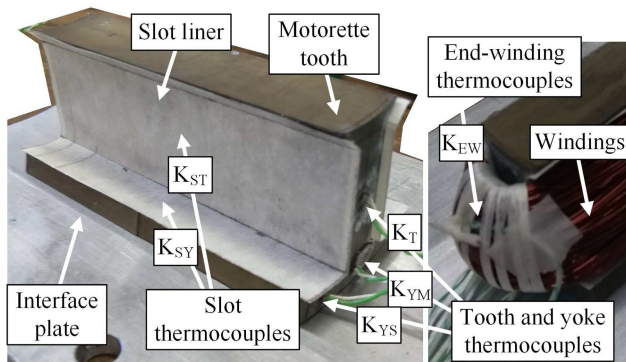
Fig. 4 *Single motorette with thermocouple positions*
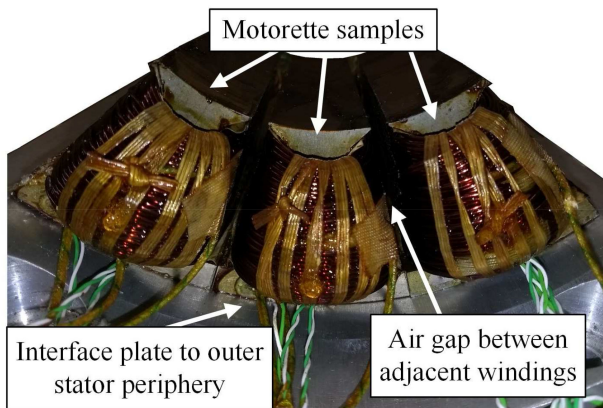
Fig. 5 *Three motorette samples, post thermocouple placement, winding and impregnation process*

Fig. 6 *Thermal chamber and test set-up*

Fig. 7 *Test assembly showing the rotor bridge*

supply will identify the differences due to the harmonic content present in the current waveform. The full procedure and results from each step are presented below. It is important that the clamped assembly presented in Fig. 7 is not altered between tests. This will ensure that the thermal interface between the motorette and interface plate remains unchanged.

4.1 DC current

The motorette samples were tested at a range of currents to thermal steady state. Thermal equilibrium was deemed to be met when end-winding temperature change was <0.5°C, over a 10-min period. The thermocouple temperature data within the motorette samples was recorded every 10 s. In addition, thermocouples were added to measure the interface plate temperature and ambient temperature within the thermal chamber. The voltage drop across the motorette and input current are recorded at the steady-state condition, to provide the total DC winding loss. The DC current is measured using a high accuracy LEM IT 400-S ULTRASTAB current transducer.

A lumped parameter-based thermal model was formulated and is based upon the geometry of the machine, and properties of the selected materials [12]. The slot region uses a cuboidal element approach, where the winding and impregnation compound are combined into a single component with separate thermal conductivities in three dimensions [13]. The interfaces between materials, such as the stator to housing, are modelled as a layer of air. Within the model, an estimation for the end-winding length is made. The winding total length was found from measurements of open-circuit resistance with a low-ohm meter. For simplicity, only the stator and water-cooled housing are modelled.

A particle swarm optimisation routine [14] and fitness function was developed to calibrate the thermal model. The fitness for each iteration of the calibration process is gauged by how close the modelled and measured temperatures are aligned (1). In (i), T_{mtk} is the recorded temperature data for one of the five regions: K_{EW}, K_{ST}, K_{SY}, K_T or K_Y, where T_{mdk} is the thermal model prediction for the same region, and K_Y is the average between K_{YM} and K_{YS}. A sixth fitness component is also introduced, (ii) which compares the predicted total loss L_{mtk}, to the measured loss L_{mdk}. The overall fitness is determined as in (iii) where a value of six represents a perfect match. Equal weighting is given to each of the six relative error components, E_{k1-6}.

$$E_{k_{1-5}} = 1 - \frac{abs(T_{mtk} - T_{mdk})}{T_{mtk}} \tag{1}$$

$$E_{k_6} = 1 - \frac{abs(L_{mtk} - L_{mdk})}{L_{mtk}} \tag{2}$$
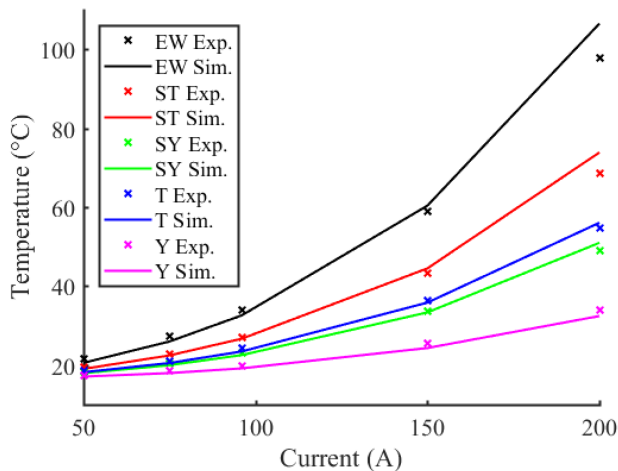
$$F = \sum_{k=1}^{6} E_k \tag{3}$$

The eight inputs to the calibration are:

- Radial S_r, tangential S_t and axial S_a thermal conductivity of the slot cuboids.
- Radial EW_r, tangential EW_t and axial EW_a thermal conductivity of the slot cuboids.

Table 2 Calibrated thermal model properties

Thermal conductivity, W/m·K						G_{ss}, μm	G_{sh}, μm
S_r (X)	S_t (Y)	S_a (Z)	EW_r (X)	EW_t (Y)	EW_a (Z)		
0.5	1	143	2.13	2.21	238	6.5	13.9

Fig. 8 *Thermal steady state temperature comparison between motorette experimental data and calibrated thermal model, for DC current*
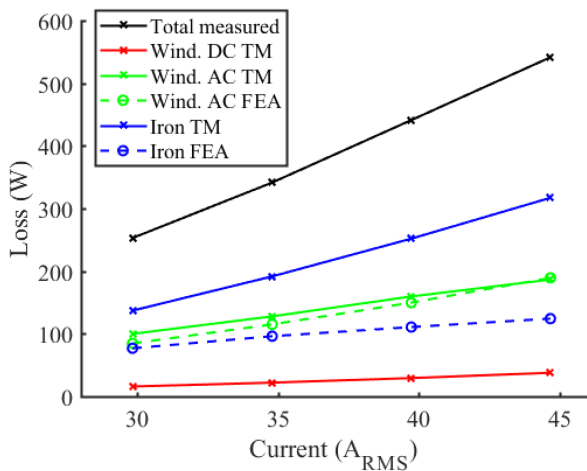
Fig. 9 *Triple motorette and rotor bridge loss at 400 Hz with sinusoid excitation. Measured total loss with estimated split using the thermal model (TM) and FEA simulation*

- Slot liner to stator effective air gap G_{ss}.
- Stator to housing effective air gap G_{sh}.

The optimal solution output from the optimisation routine is summarised in Table 2, and a comparison between the experimental data and calibrated thermal model is presented in Fig. 8. A close match is achieved, with a fitness of 5.7 out of 6, averaged across all operating points.

4.2 AC current

To provide a sinusoidal excitation with low THD, a California Instruments CSW5550 AC source has been used. Thermal steady-state measurements are taken in a similar manner to the testing with a DC excitation. However, to provide accurate loss measurements, a Fluke Norma 5000 power analyser was used, combined with a precision Fluke 150 A, 0.5 MHz, current shunt, and TL711 voltage test leads. Measurements are taken up to a maximum current of 45 A_{rms}. For the purposes of this paper, a single test frequency of 400 Hz has been selected for analysis.

The calibrated lumped parameter thermal model has been used to find an estimate for the proportion of the total loss attributed to each of the separate loss components: DC winding, AC winding,
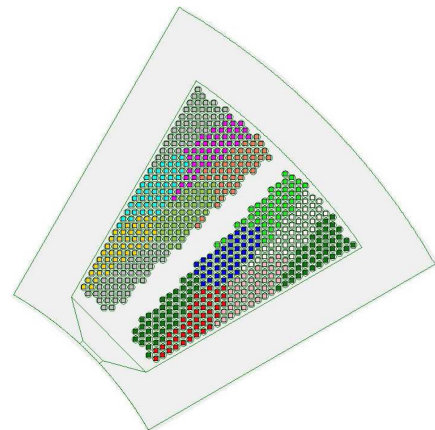
Fig. 10 *Slot cross section with conductor placement used for FEA winding loss calculation [12]*

and iron. This has been done using the same particle swarm optimisation and fitness function described by (1)–(3). However, the inputs used this time are the magnitudes of loss for each of the separate components. The optimisation will aim to find the spread of loss, which gives the closest temperature fit to those recorded from the test.

Within the lumped parameter thermal model, three heat sources are used to represent winding loss. These are split simply between the active length and the two end-winding regions. AC winding loss is added on top of the DC winding loss, for the active length source. DC winding loss is not used as an input to the optimisation, as the procedure to calculate this has been thoroughly calibrated in the previous section. The iron loss is separated into two regions: the stator tooth and stator yoke.

The result of this method is presented in Fig. 9, carried out for four steady-state measurements, at 400 Hz. The average fitness achieved was 5.8 out of 6. It is immediately apparent that the total measured loss with an AC current is significantly higher than at the equivalent DC RMS current. To aid comparison, a FEA simulation has been carried to estimate the AC winding loss, [12]. Proximity loss is highly sensitive to the lay of the conductors, particularly when winding bundles are used. The conductor layout used for this calculation is shown in Fig. 10, and approximates the winding layout expected. A close match is observed between the estimated winding loss from the thermal model method and the FEA simulation. An FEA simulation to calculate iron loss has also been carried out [12]. Here, the modified Steinmetz equation has been used [15], with iron loss coefficients calculated from the manufacturer's data sheet, with a rotating stator current and no magnets on the rotor. A significant deviation is observed and is likely due to the lamination build factor, but further investigation is required to support this.

4.3 PWM supply

A bespoke single-phase, fast switching silicon carbide-based inverter has been used to provide a PWM-based source for testing. The converter uses a half-bridge, open-loop topology, Fig. 11a, with a large split DC link capacitance to maintain the centre point voltage. A Cree CAS300M12BM2 1.2 kV 300 A half-bridge module is combined with a Cree PT62SCMD12 SiC MOSFET gate driver, Fig. 11b. The input capacitor array and bus-bar has been designed to provide low equivalent series resistance and inductance. The silicon-carbide devices are switched at 50 kHz, and a DSPACE hardware in-the-loop platform is used to control the converter.
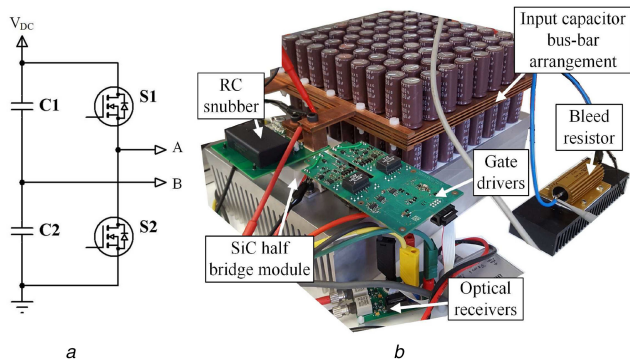
Fig. 11 *SiC inverter to provide PWM supply source,*
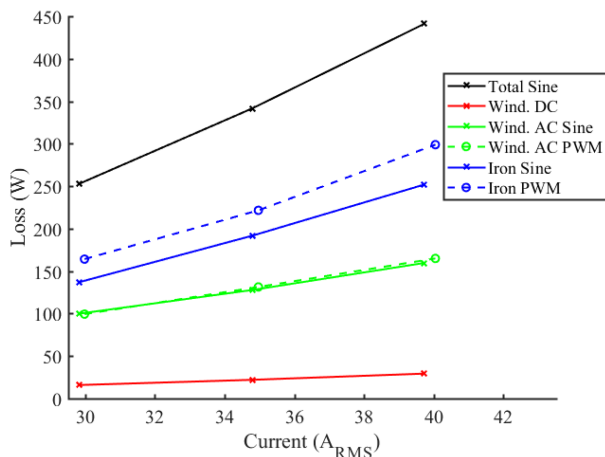*(a)* Topology and, *(b)* Labelled photograph

Fig. 12 *Triple motorette and rotor bridge loss at 400 Hz. Sinusoidal excitation versus PWM*

Steady-state thermal tests are repeated in the same manner as with the AC power supply. As expected, the loss measurements via the power analyser were identical to the low THD sinusoid measurements. However, the thermocouple temperature measurements are around 4–10% higher, at all locations and operating points. This indicates that more loss is present in the motorette sample. The same optimisation and fitting routine used to create Fig. 9 has been used to analyse the PWM supply results, except with the loss error component removed, (2). The results from this are presented in Fig. 12, and compared to the predicted loss distribution from the low THD sinusoidal tests. The average fitness achieved was 4.8 out of 5. The thermal model suggests that iron loss is increased in the motorette sample by around 15–20%, due to the PWM based supply. Whereas winding loss remains unchanged.

5 Conclusions and further work

Here, a sub-assembly-based experimental technique has been developed to study iron loss in electric machines. By combining three motorette samples and a section of a rotor, a magnetic circuit has been created which emulates the distribution of flux during normal machine operation. Steady-state thermal tests with DC

excitation provides the means to calibrate a thermal model of the machine. This thermal model has then been used to differentiate the individual components of loss present with AC excitation. A comparison of two separate tests with a low THD AC source, and a SiC-based inverter, suggests that the iron loss is increased by around 15–20%, due to the PWM-based supply, for the machine design in question.

The technique demonstrates great potential for thermal and loss analysis of a candidate machine design, prior to manufacture of the full machine. Further work will focus on supplementary experimental analysis. These will include testing of the motorette without the rotor to verify the predicted AC winding loss, using search coils to verify the flux density within the iron, investigating the cause of higher than predicted iron loss under sinusoidal excitation and repeating the analysis for different operating frequencies.

6 Acknowledgments

7 References

[1] Liu, R., Mi, C.C., Gao, D.W.: 'Modeling of eddy-current loss of electrical machines and transformers operated by pulsewidthmodulated inverters', *IEEE Trans. Magn.*, 2008, **44**, (8), pp. 2021–2028
[2] Rasilo, P., Salem, A., Abdallh, A.*, et al.*: 'Effect of multilevel inverter supply on core losses in magnetic materials and electrical machines', *IEEE Trans. Energy Convers.*, 2015, **30**, (2), pp. 736–744
[3] Xue, S., Feng, J., Guo, S.*, et al.*: 'Iron loss model for electrical machine fed by low switching frequency inverter', *IEEE Trans. Magn.*, 2017, **PP**, (99), pp. 1–1
[4] Takeda, Y., Takahashi, Y., Fujiwara, K.*, et al.*: 'Iron loss estimation method for rotating machines taking account of hysteretic property', *IEEE Trans. Magn.*, 2015, **51**, (3), pp. 1–4
[5] Gmyrek, Z., Boglietti, A., Cavagnino, A.: 'Iron loss prediction with pwm supply using low- and high-frequency measurements: analysis and results comparison', *IEEE Trans. Ind. Electron.*, 2008, **55**, (4), pp. 1722–1728
[6] Masisi, L., Ibrahim, M., Wanjiku, J.*, et al.*: 'The effect of two- and three-level inverters on the core loss of a synchronous reluctance machine (synrm)', *IEEE Trans. Ind. Appl.*, 2016, **52**, (5), pp. 3805–3813
[7] Wrobel, R., Williamson, S.J., Booker, J.D.*, et al.*: 'Characterizing the in situ thermal behavior of selected electrical machine insulation and impregnation materials', *IEEE Trans. Ind. Appl.*, 2016, **52**, (6), pp. 4678–4687
[8] Godbehere, J., Wrobel, R., Drury, D.*, et al.*: 'Experimentally calibrated thermal stator modelling of ac machines for short-duty transient operation', *IEEE Trans. Ind. Appl.*, 2017, **PP**, (99), pp. 1–1
[9] Wrobel, R., Salt, D., Griffo, A.*, et al.*: 'Derivation and scaling of ac copper loss in thermal modeling of electrical machines', *IEEE Trans. Ind. Electron.*, 2014, **61**, (8), pp. 4412–4420
[10] 'Finite element method magnetics'. 2017. Available at http://www.femm.info
[11] Goss, J., Staton, D., Wrobel, R.*, et al.*: 'Brushless ac interior permanent magnet motor design: comparison of slot/pole combinations and distributed vs. Concentrated windings'. 2013 IEEE Energy Conversion Congress and Exposition, Denver, CO, USA, 2013, pp. 1213–1219
[12] Motor-CAD: 2017. Available at http://www.motor-design.com
[13] Wrobel, R., Mellor, P.: 'A general cuboidal element for three- dimensional thermal modelling', *IEEE Trans. Magn.*, 2010, **46**, (8), pp. 3197–3200
[14] Robinson, J., Rahmat-Samii, Y.: 'Particle swarm optimization in electromagnetics', *IEEE Trans. Antennas Propag.*, 2004, **52**, (2), pp. 397–407
[15] Ionel, D.M., Popescu, M., McGilp, M.I.*, et al.*: 'Computation of core losses in electrical machines using improved models for laminated steel', *IEEE Trans. Ind. Appl.*, 2007, **43**, (6), pp. 1554–1564